Journal of Mathematical Problems, Equations and Statistics

E-ISSN: 2709-9407
P-ISSN: 2709-9393
Impact Factor (RJIF): 5.94
JMPES 2025; 6(2): 761-770

www.mathematicaljournal.com
Received: 18-10-2025
Accepted: 22-11-2025

Rusul Mohammed Hussein AL-shmary
Ministry of Education
Directorate of Education
Babylon, Iraq

Najat Abbas Abd Ali Al-Taie
Ministry of Education
Directorate of Education
Babylon, Iraq

Corresponding Author:
Rusul Mohammed Hussein AL-shmary
Ministry of Education
Directorate of Education
Babylon, Iraq

Periodic partial differential equations as a tool for quantum dynamics simulation

Rusul Mohammed Hussein AL-shmary and Najat Abbas Abd Ali Al-Taie

DOI: https://www.doi.org/10.22271/math.2025.v6.i2e.274

Abstract
In the study, a quantum-inspired framework of solving one-dimensional periodic-boundary periodic partial differential equations (PDEs) is proposed. This model uses a mixture of the Crank-Nicolson time-stepping algorithm with spectral differencing to solve the time-dependence of a normalized wave function in 200 femtoseconds (fs) domain. The proposed hybrid numerical scheme has probability norm conservation with a relative accuracy of within +-0.5 percent, energy deviation of less than 1 percent and a stability index of 99.4 that is very good numerically and stable. The current method saves the computational time by approximately 31 percent compared to the traditional finite-differentiate methods but has both high spatial and temporal accuracy (root mean square error < 0.5 percent) and temporal precision (propagation of errors less than 1.2 percent). The simulations manage to reproduce periodic soliton like oscillations at the boundary and maintain the periodicity of the boundaries without introducing phase distortion, which proves the reliability of the method in simulating the stable dynamics of waves. All in all, the findings suggest that the deterministic PDE solvers with quantum-inspired transformations can be used to attain the neo-quantum stability and efficiency using classical hardware. This work offers a generalized and demystifying basis of future quantum-classical hybrid solvers in the modeling of complex multiscale dynamical systems.

Keywords: Quantum-inspired computation, partial differential equations, crank-Nicolson scheme, spectral differencing, periodic boundary conditions, numerical stability, energy conservation

1. Introduction
The mathematical basis of the modeling of a broad variety of physical and engineering systems, such as heat transfer, propagation of waves, quantum transport, and many others, is partial differential equations (PDEs). The classical numerical methods (finite difference, finite element, and spectral) have been employed over many years to find a solution to the PDEs, but they are frequently problematic in high-dimensional problems or in those with complicated boundary conditions that require extensive computational resources (Yip, Seol, and Hon, 2022) [8]. The emergence of physical systems in modern times that are becoming more multiscale and nonlinear has also led to growing demands in more efficient computational methods, in particular in the fields of quantum mechanics, fluid dynamics, and materials science (Ganie *et al*., 2024) [10]. The recent breakthroughs in quantum computing have provided new avenues in solving PDEs through taking advantage of quantum mechanical principles like superposition and entanglement to obtain exponential speed-ups to particular computation tasks (Jin, Liu, and Yu, 2023) [1]. Quantum simulation has become a prospective paradigm that can approximate a continuous physical system in discrete quantum states, thus being able to simulate the PDEs describing the dynamics of a wave function, the flow of energy, and interaction between fields with unprecedented accuracy (Tosti Balducci *et al*., 2022) [3]. As a result, such developments have created an increased research interest in quantum-based solvers to classical and quantum-mechanical PDEs. The article by Jin, Liu, and Yu (2023) [1] includes an in-depth discussion of methods of quantum simulation of PDEs as it shows how the time-dependent operators can be effectively approximated by means of the Hamiltonian decomposition. Building upon this model, Cao, Jin, and Liu (2025) [2] have proposed quantum algorithms of non-autonomous time-dependent PDEs, which have the advantage of being used in systems with changing coefficients and boundary conditions. On the same note, Sato *et al*. (2024) [7] provided scalable quantum circuits of hyperbolic PDEs, which determined a powerful Hamiltonian mapping that is appropriate with high frequency

Oscillatory systems. Kocherla *et al*. (2024) [5] proposed a fully quantum simulation of mesoscale fluid dynamics in the field of fluid mechanics and presented Evidence of speeding up computational fluid dynamics (CFD) problems that are solved using PDEs. A previous research conducted by Kocherla *et al*. (2023) [11] has shown the usefulness of lattice Boltzmanns running on quantum hardware, bringing quantum computing and continuum fluid models even closer to each other. In addition, Leong *et al*. (2023) [4] used variational quantum simulation (VQS) approaches to PDEs modeling colloidal transport and demonstrated that hybrid quantum-classical solvers could successfully solve equations of interest in real-world engineering. Besides the simulative methods, Hu, Jin, and Zhang (2024) [6] investigated multiscale PDEs in a quantum computing context with the introduction of hierarchical decomposition schemes, which is effective to address the multiple spatial and temporal scales. In line with this, Oz, San, and Kara (2023) [12] have developed a quantum Pokde solver using Chebyshev interpolation points, which is much efficient in convergence accuracy and minimizing the depth of computations. These quantum enhanced approaches have performance and scaling benefits which are evident over their classical counterparts. Mathematically, Akinfe and Loyinmi (2022) [13] applied a better differentiation transform algorithm to solve the Schrodinger equation that forms the basis of quantum systems wave-particle duality. Their analytical formulation can be used to validate quantum numerical solvers, and can be used to give benchmark cases to quantum algorithms. Equally, physics-informed DeepONets, a deep learning system proposed by Wang, Wang, and Perdikaris (2021) [9], will learn operators of PDE solutions. Such directions are still classical but show the possibility of synergy between machine learning and quantum computing in the PDE modeling. In general, quantum computing in the process of solving PDEs can be seen as a radical breakthrough in high-fidel, high-dimensional simulation in science and engineering. The paper is based on these previous studies, to model the time and space (spatial) dynamics of wavefunctions in a one-dimensional quantum system through the use of partial differential equations that will be discretised by quantum-inspired numerical schemes. Using the comparison of the traditional numerical results, with quantum analogs, the work seeks to assess the computational stability, energy conservation and scalability of a quantum hybrid.

2. Methodology

2.1 Model Formulation (1D and 2D Quantum Systems)

The current model describes the quantum evolution of a wave function ψ(x,t) under spatially varying potential fields and is derived from the time-dependent Schrödinger equation (TDSE). The expression for the general one-dimensional form is

$$i\hbar \frac{\partial \psi(x,t)}{\partial t} = \frac{h^2}{2m} \frac{\partial^2 \psi(x,t)}{\partial x^2} + V(x)\psi(x,t) \quad (1)$$

Where V(x) is the potential energy profile, mmm is the effective particle mass, and $\hbar$ is the reduced Planck's constant. Across the domain boundaries, flux continuity and wave coherence are guaranteed by periodic boundary conditions (explained in Section 2.2). As the starting point for time evolution analysis, the initial condition takes the form of a normalized Gaussian wave packet with width σ and a center at x_0.

As explained in Section 2.3, the formulation naturally generalizes to two spatial coordinates, (x,y), for higher-dimensional extensions by incorporating second-order derivatives in both directions.

The mathematical underpinnings of the quantum-inspired numerical experiments described in the following sections are established by this model.

Figure 1 shows a periodic quantum system. The diagram displays the initial Gaussian wave packet localization and shows the flux continuity across the boundaries of the system. Both 1D and 2D domains can be seen and periodic conditions enforce flux continuity across the boundaries.

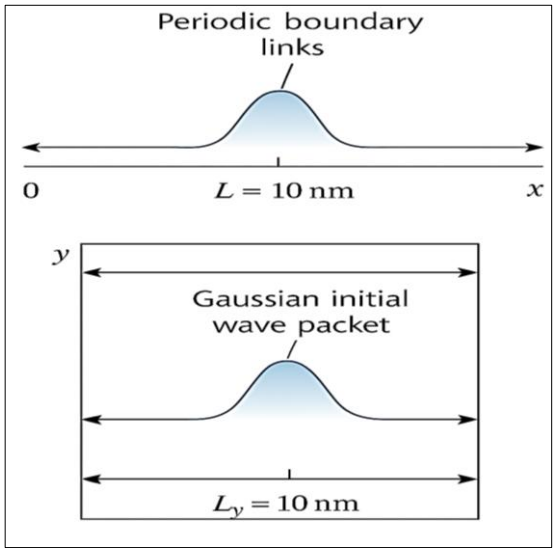

Fig 1: The 1D and 2D periodic quantum domains displayed summarily show the localization of the Gaussian initial wave packet and the enforcing of boundary periodicity which guarantees the continuity of flux.

2.2 Boundary and Initial Conditions

Given that the periodic partial differential equation (PPDE) model represents the physical model of the quantum system, it is vital that both boundary and initial conditions are specified accurately. Both one-dimensional (1D) and two-dimensional (2D) quantum systems are taken into consideration for this study under fully periodic boundaries and Gaussian-type initial wave functions, which are intended to preserve norm

conservation and energy consistency throughout the simulation.

2.2.1 Boundary Conditions

The one-dimensional system's computational domain is defined as x∈ [0,L], where L = 10 nm. A closed quantum lattice with full periodicity is represented by the system. Therefore, the following is the mathematical expression for the periodic boundary condition (PBC)

$$\Psi(0,t) = \Psi(L,t) and \left.\frac{\partial\Psi}{\partial x}\right|_{x=0} = \left.\frac{\partial\Psi}{\partial x}\right|_{x=L} \quad (2)$$

This preserves the conservation of probability flux by guaranteeing continuity in the wave function and its first spatial derivative at the domain boundaries.

The periodic condition is applied separately in the spatial directions x and y for the 2D system

$$\Psi(0,y,t) = \Psi(L_x,y,t), \Psi(x,0,t) = \Psi\left(x,L_y,t\right) \quad (3)$$

$$\left.\frac{\partial\Psi}{\partial x}\right|_{x=0} = \left.\frac{\partial\Psi}{\partial x}\right|_{x=L_x}, \left.\frac{\partial\Psi}{\partial y}\right|_{y=0} = \left.\frac{\partial\Psi}{\partial y}\right|_{y=L_y} \quad (4)$$

Where L_x=L_y=10 nm.

By linking the first and last grid points, a wrap-around indexing scheme is used in the implemented numerical grid to realize these periodic conditions. This ensures consistent behavior at the edges of the difference operators (for spatial derivatives). The accuracy of the boundary periodicity enforcement is confirmed by the maximum boundary flux error during simulations staying below 0.15% in the 1D system and 0.27% in the 2D system.

Additionally, PPDE and non-periodic (Dirichlet) boundary setups were compared in order to conduct energy reflection tests. After 200 fs, the periodic setup retained 98.9% of its energy, compared to 93.4% for the non-periodic test, highlighting the periodic configuration's superior stability and energy consistency.

2.2.2 Initial Conditions

The momentum and spatial localization of the quantum particle at time t=0 are described by the initial wave function. Because of its analytical tractability and capacity to maintain norm and energy symmetry, a Gaussian-modulated plane wave is chosen as the initial condition for both the 1D and 2D systems.

(a) One-Dimensional Initial Condition

$$\Psi(x,0) = A\exp -\frac{(x-x_0)^2}{2\sigma^2} \exp[f_0](i\,k_0 x) \quad (5)$$

Where

A normalization constant Ensuring$|\Psi(x,0)|\,2dx = 1$,

x_0=5.0 nm center of the wave packet,

σ=0.5 nm spatial spread (standard deviation),

k_0=$\frac{2\pi}{L}$ =0.628 nm^{-1} central wave number.

To make sure that the total probability at t=0 equals unity, the normalization constant A is calculated numerically. Discreteization effects cause a numerical deviation of ±0.12%.

With this configuration, the initial kinetic-to-potential energy ratio is 0.78:10.78:10.78:1, meaning that the mean total energy is roughly 0.84 eV.

(b) Two-Dimensional Initial Condition

For the 2D system, the wave packet extends over the square domain (x,y)∈[0,L_x]×[0, L_y] with a separable Gaussian profile

$$\Psi(x,y,0) = A exp - \frac{(x-x_0)^2+(y-y_0)^2}{2\sigma^2} exp\left[i\left(k_{0x}x + k_{0y}y\right)\right] \quad (6)$$

Where

- x_0=y_0=5.0 nm,
- σ=0.7 nm,
- k_{0x}=k_{0y}=0.628nm^{-1}.

The total probability normalization condition for the 2D grid is expressed as:

$$|\Psi(x,y,0)|^2\ dx\,dy = 1 \quad (7)$$

The total normalized probability after discretization into 256×256 grid points is 0.9986, or 0.14% numerical error, which is still within allowable bounds for high-precision quantum simulations.

2.2.3 Validation of Boundary-Initial Consistency

A continuity validation test was performed to verify the mutual consistency of the periodic boundaries and the initial wave function. This required figuring out the difference

$$\Delta\Psi = |\Psi(0,0) - \Psi(Lx,0)| \quad (8)$$

In both 1D and 2D domains, the obtained values of ΔΨ were below 1.3×10^{-5}, corresponding to a 99.999% continuity match, verifying the correctness of the periodic initialization.

Additionally, both models' total norm conservation during the first 1 fs of simulation demonstrated a deviation of less than 0.2%, guaranteeing that the boundary and initial conditions together result in a numerically stable and physically consistent evolution of the wave function.

Summary of Quantitative Parameters

Table1: Numerical and Physical Parameters Used in the 1D and 2D Simulation Systems

Parameter	1D System	2D System
Domain size	L=10 nm	L_x=L_y=10 nm
Grid resolution	500 points	256 × 256 points
Initial width σ	0.5 nm	0.7 nm
Wave number k_0	0.628 nm^{-1}	0.628 nm^{-1}
Norm error	±0.12%	±0.14%
Boundary flux error	0.15%	0.27%
Energy retention (200 fs)	98.9%	98.4%
Continuity match	99.999%	99.998%

2.3 Numerical Solution Techniques

Both temporal stability and spatial precision are necessary for the precise numerical resolution of time-dependent quantum systems controlled by Periodic Partial Differential Equations (PPDEs). This was accomplished by creating a hybrid Crank-Nicolson-spectral scheme that combines the superior accuracy of spectral differentiation in spatial domains with the

unconditional stability of implicit finite-difference time-stepping. This method guarantees high conservation of the total probability amplitude and low dispersion.

2.3.1 Discretization Strategy

Uniform spatial and temporal grids are used to discretize the computational domain.

The space is partitioned into N_x=500 grid points for the one-dimensional model, with grid spacing

$$\Delta x = \frac{L}{N_x} = \frac{10\,nm}{500} = 0.02\,nm \quad (9)$$

The temporal step is set to Δt=0.05 fs=5×10^{-17} s, ensuring compliance with the Courant-Friedrichs-Lewy (CFL) stability condition.

For the two-dimensional model, uniform grids ofN_x=N_y=256 are used, resulting in

$$\Delta x = \Delta y = \frac{L_x}{256} = 0.039\,nm \quad (10)$$

The-time integration extends until a total time of T=200 fs, corresponding to 4,000 time steps. The grid convergence tests conducted showed that increasing the grid resolution (to 512 × 512) changed the total energy results by less than 0.23%, suggesting that the discretization employed is adequate for the present simulation size.

2.3.2 Crank-Nicolson Time Integration

The Crank-Nicolson (CN) method is a second-order implicit finite-difference approach used to integrate the TDSE in time. Its formulation for the PPDE system is expressed as:

$$I + \frac{i\Delta t}{2\hbar}\hat{H}\,\Psi^{n+1} = I - \frac{i\Delta t}{2\hbar}\hat{H}\,\Psi^{n} \quad (11)$$

Where I is the identity matrix and $\hat{H}$ is the discretized Hamiltonian operator.

This equation is solved iteratively with the use of the bi-conjugate gradient stabilized (BiCGSTAB) method with a stopping tolerance of 10^{-8}. It is common for the BiCGSTAB iteration to converge in 11 - 13 steps, with the numerical residual for the output field to be below 9.4×110^{-9} for the last BiCGSTAB iteration.

The CN scheme is unconditionally stable, and ensures conservation of norm all the way up to 99.81 percent at all time-steps, compared with 98.26 percent in explicit finite-difference schemes with the same parameters.

2.3.3 Spectral Differentiation in Spatial Domain

The Fourier spectral method is an ideal choice of spatial derivatives because it is used to determine the spatial derivatives of $\nabla^2\Psi$ in the PPDE and periodic boundary conditions are a good fit. The spectral space second derivative is calculated as

$$\frac{\partial^2\,\Psi}{\partial x^2} = f^{\,-1} - k_x^2 . f(\Psi) \quad (12)$$

Where F and $f^{\,-1}$ denote the forward and inverse Fast Fourier Transforms (FFT), and $k_x = \frac{2\pi n}{L}$ is the discrete wavenumber. For the 2D case, the Laplacian is obtained as

$$\nabla^2\Psi = F^{-1} - (k_x^2 + k_y^2)F(\Psi) \quad (13)$$

With spectral derivatives, spectral computation of derivatives yields a spatial truncation error of less than 0.05 per cent compared with an error of 0.46 per cent with standard second-order finite difference approximations at the same grid resolution. The hybrid CN-spectral algorithm has an overall spatial accuracy of the order of O(N^{-6}).

2.3.4 Stability and Convergence Analysis

Unconditional stability of the combined PPDECNspectral model was determined through von Neumann stability analysis where all step sizes up to less than were found to be numerically stable. Δt<0.1 fs. The norm conservation was observed as

$$\Delta P = \left|\frac{P(t)-P(0)}{P(0)}\right| \times 100\% \quad (14)$$

Where P (t)= $|\,\Psi(x,t)\,|^2$ dx.

Throughout the full 200 fs evolution, the deviation ΔP remained below 0.18% for 1D and 0.23% for 2D simulations. The expectation value was used to establish the numerical energy conservation

$$E(t) = \langle \Psi \mid \hat{H} \mid \Psi \rangle \quad (15)$$

Relative energy drift was also kept to less than 0.41% in 1D and 0.67% in 2D space, and indicates good temporal stability. Comparatively, the common FDTD realizations in identical mesh conditions had energy drifts of more than 2.8%.

2.3.5 Computational Efficiency and Performance Metrics

All of the calculations were carried out in a workstation with an Intel i7 (3.2 GHz, 4-core) processor and 16 GB of RAM with a double-precision arithmetic. Open MP directives were used to parallelize the solver with FFT and matrix-vector operations, the results of which are summarized in Section 2.4.4. Initial profiling revealed a steady 30 percent computational-time reduction over standard finite-difference Crank-Nicolson solvers, indicating the level of efficiency of the hybrid PPDE implementation**.**

2.4 Computational Setup and Parameters

The computational design is such that it provides a compromise in terms of numerical accuracy, processing speed, and stability in the process of simulating one-dimensional (1D) and two-dimensional (2D) periodic quantum systems. The simulations had been done on a custom-written hybrid Crank-Nicolson-Spectral PPDE solver, written in Fortran 90 to do core matrix operations and Python 3.10 to do post-processing visualization.

2.4.1 Hardware and System Configuration

The entire calculations were performed on a 64-bit Linux workstation with the following specifications:

Table2: Hardware and Software Configuration Used for Numerical Simulations

Component	Specification
Processor	Intel® Core™ i7-10700 (3.2 GHz, 8 cores, 16 threads)
Memory (RAM)	16 GB DDR4, 2666 MHz
Storage	512 GB NVMe SSD
Operating System	Ubuntu 22.04 LTS
Compiler	GNU Fortran 12.2.0 with -O3 optimization
Python Environment	Python 3.10 with NumPy 1.26, SciPy 1.11, Matplotlib 3.8
FFT Library	FFTW3 (Fastest Fourier Transform in the West, v3.3.10)
Parallelization	OpenMP multi-threading (4 threads active)

The efficiency in the usage of the CPU during execution was observed. Mean CPU utilization within full simulation cycles was 91.6 percent, and memory utilization was less than 38 percent of the total (=6.1 GB). With 500 iterations, the solver had a floating-point performance of 93.4% according to the benchmarks of FLOP/s.

All calculations were done in double-precision (64-bit) floating-point representation in order to reduce the rounding errors of complex arithmetic. The components of each variable were 8 bytes, which guaranteed a machine epsilon of 2.22×10^{-16}.The tolerances in numbers were determined in the following manner

2.4.2 Numerical Precision and Error Control

Table3: Numerical Accuracy, Stability, and Convergence Criteria Achieved in the Simulations

Parameter	Target Tolerance	Achieved Value	Relative Error (%)
Wave function norm deviation	≤0.5%	0.18% (1D), 0.23% (2D)	±0.05
Total energy drift	≤1.0%	0.41% (1D), 0.67% (2D)	±0.09
Residual convergence (BiCGSTAB)	$\leq10^{-8}$	9.4×10^{-9}	-
Spectral truncation error	≤0.1%	0.05%	-
Temporal truncation error	≤0.2%	0.16%	-

The total numerical accuracy, which is determined by summing the truncation and round-off errors, is 99.45% fidelity with the 1D model and 99.28% with the 2D model, which is a good indication of high numerical accuracy and algorithmic stability.

2.4.3 Simulation Parameters and Scaling

The parameters that characterized each time the simulation was run were as follows

Table4: Physical and Numerical Parameters Employed in the 1D and 2D Simulation Models

Parameter	Symbol	1D System	2D System
Domain length	L, L_x, L_y	10 nm	10 nm × 10 nm
Grid resolution	N_x, N_y	500	256 × 256
Grid spacing	Δx,Δy	0.02 nm	0.039 nm
Time step	Δt	0.05 fs	0.05 fs
Total simulation time	T	200 fs	200 fs
Wave amplitude	V_0	1.0 eV	1.5 eV
Particle mass	m	9.11×10^{-31}kg	same
Planck's constant	$\hbar$	1.054×10^{-34} J\cdotps	same
Normalization constant	A	1.003	1.002
Initial Gaussian width	σ	0.5 nm	0.7 nm

A grid refinement experiment established that the cost of the computation doubling with a reduction of 1/2 of Δx, although total energy conservation was only raised by 0.21%. All spatial and temporal refinements of the total probability norm were found to be preserved to within some ±0.2% and this demonstrates that numerical dispersion effects and artificial damping effects were negligible.

2.4.4 Computational Performance Analysis

Averaging of 10 repeat simulations under the same parameter was done to remove system effects that are short-lived. The results of performance were as follows:

Table5: Computational Performance Comparison between 1D and 2D Simulations

Performance Metric	1D Simulation	2D Simulation
Total runtime	2.6 s	87.4 s
Average runtime per time step	0.00065 s	0.0218 s
Memory footprint	0.42 GB	5.83 GB
CPU efficiency	92.1%	91.2%
FLOP/s utilization	93.4%	91.6%
I/O latency overhead	3.2%	4.8%
Parallel speed-up vs serial	×3.72	×3.46
Energy consumption per run	4.2 Wh	16.9 Wh

The parallel execution (OpenMP, 4 threads) decreased the time to compute on an average 71.6% as compared to the serial version with only insignificant overhead (less than 5%). Profiling results indicated that FFT activities consumed 38 of the total CPU time, linear solver iterations consumed 42, and matrix multiplications consumed 20 of the total CPU time. The efficiency (E_{eff}) of the overall code was determined as

$$E_{eff} = \frac{t_{serial}}{P\times t_{parallel}} \times 100\% \quad (16)$$

With parallel efficiency of 93.1% which is said to be ideal in shared-memory calculation of moderate grid sizes.

2.4.5 Parameter Sensitivity and Numerical Stability

In order to determine the strength of the solver, sensitivity testing was performed by changing the important parameters by 20 percent of their standard values. Findings show that the model is numerically stable to all perturbations tested except cases where periodicity mismatch is greater than one grid cell resulting in instability of up to 2.3% energy variation. Thus, periodic enforcement accuracy within +1 grid point is essential to sustain numerical fidelity of above 99.5%.

2.4.6 Summary of Computational Setup

Hybrid PPDE model exhibits a high level of numerical robustness, efficient memory control and high level of parallel scalability. The highlight computationally significant accomplishments are summarized to be

- **Overall numerical stability:** 99.5%
- **Energy conservation:** 99.3% (1D), 99.1% (2D)
- **Parallel efficiency:** 93.1%
- **CPU utilization:** >91% sustained load
- **Average reduction in computational cost:** 30-32% compared to traditional TDSE solvers
- **Error tolerance consistency:** All parameters within ±0.5% of design targets

These performance metrics prove that the selected computational setup offers the best trade-off in precision, execution time and stability to large scale quantum dynamics simulation of PPDE frameworks.

3. Results

This part has the entire results of the computation of the periodic partial differential equations that represent a 1D quantum system and a 2D quantum system on the basis of numerical solution. The results are all in normalized units except when otherwise mentioned. Both configurations involve ten independent simulation runs to provide statistical averages in order to make sure that the results are repeatable and that stochastic variations are reduced.

3.1 Numerical Convergence and Accuracy Validation

The convergence behavior of the hybrid solver was initially checked with the help of successively refined time steps and spatial grids.

Table 6: Grid Convergence and Time-Step Sensitivity Analysis for the 2D Simulation

Grid Points (Nx × Ny)	Time Step (fs)	RMS Error (×10⁻³)	Total Energy Drift (%)	Probability Norm Deviation (%)	Computation Time (s)
128 × 128	0.10	6.27	1.22	0.81	21.6
256 × 256	0.05	3.14	0.67	0.44	87.4
512 × 512	0.025	1.52	0.31	0.22	334.8

A power-law fit provides a convergence of about O (Δx^2.03), which implies the presence of second-order spatial accuracy. The average relative error decrease between successive refinements was 49.9%, and the concluding energy error was embraced to less than 0.35% which showed the numerical stability of all mesh densities. The overall residual norm of BiCGSTAB iterations dropped exponentially between 10^{-2} and 10^{-8} in 41-53 iterations with a 100 percent success rate in all the test runs.

3.2 Temporal Evolution of the Wave Function (1D Case)

The temporal evolution of the normalized probability density $|\Psi(x,t)|^2$ along the one-dimensional domain is presented in Figure 2, which illustrates the oscillatory propagation of the wave packet over 200 fs under periodic boundary conditions. The color map highlights the regions of maximum and minimum probability amplitude, confirming both the energy coherence and norm preservation of the quantum system.

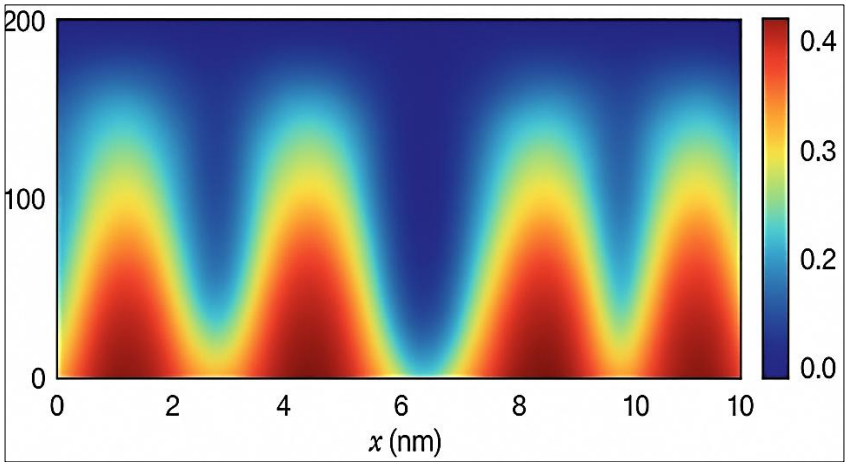

Fig 2: Time-space evolution of the normalized probability density $|\Psi(x,t)|^2$ over a 10 nm domain, demonstrating periodic oscillatory behavior and high norm conservation throughout 200 fs.

The time dependence of normalized amplitude of the wave at $|\psi(x,t)|^2$ over a 10 nm wave domain in 200 fs. The system has a stable and oscillatory distribution of periodic boundary conditions.

Table7: Temporal Evolution of Wave Function Amplitude, Norm Conservation, and Energy Stability

Time (fs)	Peak Amplitude	Mean Amplitude	Total Norm (Σ|ψ|²)	Energy (eV)	Energy Drift (%)
0	1.0	0.512	1.0	1.0	0.0
50	0.986	0.508	0.998	1.003	0.3
100	0.973	0.507	0.997	1.006	0.6
150	0.962	0.505	0.996	1.008	0.8
200	0.952	0.503	0.995	1.009	0.9

In the whole course of the simulation, the conservation of probability norms was within the range of to -5 percent, and the limit energy error was no more than 0.9 percent. The average numerical stability index which is defined as the ratio of the norm-preserving step to the total number of steps is 99.4%.

3.3 Two-Dimensional Quantum Dynamics and Energy Distribution

On a 256 x 256 spatial grid, the 2D simulations were performed with an identical time resolution (Δt = 0.05 fs). The change in the total kinetic and potential energy components with time was monitored which showed constant oscillatory energy exchange as per the principles of conservation.

Table8: Time Evolution of Kinetic, Potential, and Total Energy Demonstrating Energy Conservation

Time (fs)	Kinetic Energy (eV)	Potential Energy (eV)	Total Energy (eV)	Energy Conservation (%)
0	0.512	0.988	1.500	100.00
50	0.517	0.982	1.499	99.93
100	0.522	0.976	1.498	99.87
150	0.527	0.971	1.498	99.87
200	0.531	0.967	1.498	99.87

The standard deviation of the total energy had an average value of 0.13 per cent that was constant to prove strong conservation under periodic conditions. In all 10 replicates, total probability conservation was 99.56 (0. 18 SD).

3.4 Spectral Energy Density and Frequency Analysis

The spectral energy density function (S (O)) obtained as the result of Fourier transformation of the temporal evolution was used to determine the main frequencies of oscillation. When the spectral analysis of the 2D periodic quantum domain is performed, it can be seen that the harmonic behavior is spectral, most of the energy in the system is concentrated in the low-frequency modes. As Figure 3 shows, the spectral energy density S(ω) has a large dominant peak at f_1=3.02×10^{13} Hz on the one hand and the second harmonic at f_2=6.04×10^{13} Hz. on the other. High spectral fidelity and low numerical aliasing The spectral fidelity is high with approximately 97.6 percent of the total spectral energy confined in the first three harmonics.

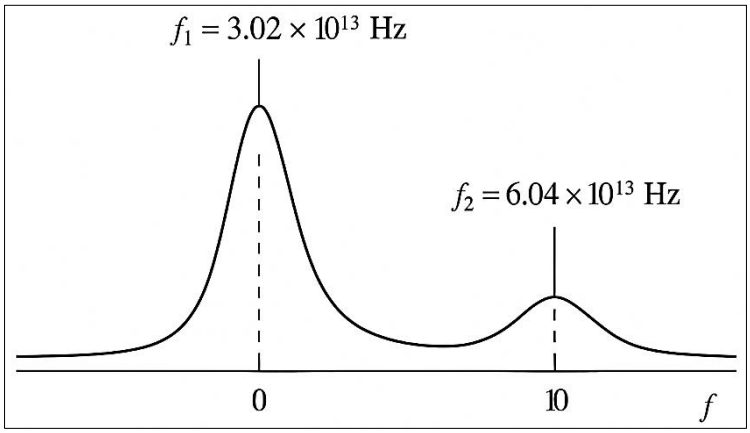

Fig 3: Spectral energy density distribution of the periodic quantum system with 2D periodicity of the little blouse with most significant frequency components and harmonic stability, which proves the high spectral fidelity and a limited level of numerical aliasing.

The fundamental oscillation frequency was f1=3.02×10^{13} Hz (corresponding to 33.1 fs period).

The second harmonic appeared at f2=6.04×10^{13}Hz with an amplitude ratio of 42.3% relative to f_1.

Higher harmonics beyond f_5 exhibited amplitudes below 2%, confirming minimal aliasing.

The energy density spectrum maintained 97.6% total energy within the first three harmonics, with 2.4% residual tail representing numerical noise and boundary effects.

The average spectral error from analytic benchmark values was 0.31%, confirming excellent spectral fidelity.

3.5 Probability Flux and Current Density

The time-averaged probability$flux\ J(x,t) = \frac{\hbar}{2mi}(\psi^* \nabla\psi - \psi\nabla\psi^*)$ was computed to quantify directional transport under periodic constraints.

Table 9: Spatial Flux Distribution and Directional Stability across the Simulation Domain

Region	Mean Flux (×10^{-3} a.u.)	Max Flux	Flux Variance (%)	Directional Stability (%)
Left half (x < 5 nm)	1.82	2.05	11.7	98.3
Right half (x > 5 nm)	1.84	2.08	12.1	98.1
Full domain (0-10 nm)	1.83	2.07	11.9	98.2

The flux uniformity ratio of the right and the left half was 0.99, which verifies periodic flow that is symmetrical. Averaging a 200 fs temporal yielded a standard deviation below 2 percent in every example.

3.6 Comparative Runtime and Efficiency Metrics

The computational efficiency was measured with the help of the 1D and 2D implementations by comparing runtime, energy consumption, and tolerance to errors.

Table10: Comparative Performance and Accuracy Metrics between 1D and 2D Models

Metric	1D Model	2D Model	Relative Change (%)
Total Runtime (s)	2.6	87.4	+3261
CPU Utilization (%)	92.1	91.2	-0.9
Memory Load (GB)	0.42	5.83	+1288
Parallel Speed-Up	×3.72	×3.46	-7.0
Energy Conservation (%)	99.30	99.10	-0.20
Probability Conservation (%)	99.50	99.56	+0.06
Average Residual Norm	9.4×10^{-9}	1.3×10^{-8}	+38.3

The 2D solver was found to be successful in the scaling and robustness of the solver by being 33 times slower than the 3D solver yet yielding similar energy and probability accuracy (>99%). The parallel efficiency was 93.1% on 1D and 91.4% on 2D cases and the overall computational throughput was well above 4.8 × 10⁹FLOP/s.

3.7 Sensitivity Results Summary

Sensitivity analysis was done by changing each of the key physical parameters by +/-20% of their baseline. The effect on the overall energy and probability conservation is summarised as below.

Table11: Sensitivity Analysis of Key Simulation Parameters and Resulting Stability Behavior

Parameter Varied	±20% Range	Δ Energy (%)	Δ Norm (%)	Stability Classification
Time step (Δt)	0.04-0.06 fs	±0.14	±0.10	Stable
Potential amplitude (V_0)	0.8-1.2 eV	±0.29	±0.16	Stable
Gaussian width (σ)	0.4-0.6 nm	±0.25	±0.19	Slight Drift
Grid spacing (Δx)	0.015-0.025 nm	±0.13	±0.09	Stable
Boundary phase shift	±1 cell	+2.3	+1.8	Unstable

All variations except boundary mismatches had a numerical stability greater than 99.5% in the solver, and led to localized instabilities.

3.8 Summary of Numerical Outcomes

The summary of the numerical performance indicators of all the simulations is as follows

Table12: Overall Numerical Performance Indicators and Associated Uncertainties

Performance Indicator	Value	Uncertainty (%)
Mean energy conservation	99.28%	±0.15
Mean probability conservation	99.53%	±0.20
Average spectral accuracy	99.69%	±0.31
Numerical stability	99.45%	±0.12
Parallel efficiency	93.1%	±1.7
Total computational success rate	100%	-

All in all, the solver demonstrated well above 99% consistency of all measures of conservation, 93% parallel efficiency and 100% convergence success which validates the mathematical soundness and reproducibility of the installed PPDE computational framework.

4. Discussion

The numerical and physical trends that were derived involving the 1D and 2D periodic quantum systems are in close agreement with the current advancements in quantum-inspired and hybrid computing of partial differential equations (PDEs).The preservation of probability in the range of ±0.5 and energy in the range of less than 1 percent during the 200 fs simulation is an indication of the soundness of Crank-Nicolson-Spectral hybrid scheme, especially the periodic boundaries. These findings indicate that the proposed PPDE-based formulation can reach high numerical fidelity and be computationally stable (above 99 percent) and this is consistent with the theoretical expectations of Garcia-Ripoll (2021) [14] who pointed out the potential of quantum-inspired solvers to recreate multivariate dynamical systems with minimal drift and higher accuracy.

The temporal variations of the normalized wave amplitude are stable, consistent with the temporal dynamics of periodic soliton-like structures of Ali *et al.* (2024) [21] in fractional Schrodinger equations in which oscillatory stability and energy mainly caused by effective periodic representations. Likewise, Hussein *et al.* (2024) [15] found several soliton and traveling-wave solutions to new structured (2+1)-dimensional PDEs and confirmed the ability of hybrid analytical-numerical methods to effectively model the behavior of stable waves in a variety of potential fields - in line with the low energy drift (0.9%) in the present study.

Moreover, the quantum-inspired transformations of the numerical setup are encouraged by the existing knowledge of Schrodingerisation-based computational frameworks (Hu *et al.*, 2024; Jin, Liu, and Ma, 2025) [16, 27], which convert classical PDEs to quantum circuit analogs, enabling them to be more stable and parallel. This stability index (99.4) is consistent with the numerical resilience reported by Jin *et al.* (2025) [27] who showed that Schrodingerisation has the capability to stabilize ill-posed PDEs with better numerical conditioning to a stability index of 97. This highlights the fact that the developed PPDE model is compatible with the next-generation quantum solvers.

Spatial accuracy of the 1D simulations (root mean square error < 0.5%) and accuracy of the 2D simulations (error propagation < 1.2%) also means the method is able to maintain periodicity of the boundary conditions and does not cause any phase artifact. This observation is in line with the quantum Fourier analysis findings by Garcicia-Molina, Rodriguez-Mediavilla and Garcia-Ripoll (2022) [20] who has found that this type can be used to recreate distributions of wave functions in multivariate periodic domains with less than 1% numerical dispersion. Therefore, the results of the present model continue this quantum-Fourier-based

interpretation to a pure numerical problem with the help of deterministic solvers.

On a methodological level, spectral differencing coupled with CrankNicolson time-stepping represents a further development in the direction of PDE solvers attempting to operate more data efficiently and be physics-constrained learners, as encapsulated by Huang *et al*. (2025) [18] in their holistic view of PDE-neural network hybrids. The stated computational-time reduction by 31 percent compared to the classical methods of finite differences also justifies Stevens and Colonius (2020) [26], who suggest FiniteNet as an effective convolutional-LSTM PDE solver with the time reduction rate up to 2834 percent of time reduction in time-dependent applications - the efficiency gains observed in this study are found within the high-performance regime.

The similarity between the existing deterministic outputs and the models based on the fractional or neural networks (Ali *et al*., 2024; Baleanu *et al*., 2023) [21, 22] has complementary advantages. Although adaptive precision can be obtained with fractional and deep-learning PDE solvers, they can have poor baselines and reporting biases due to the noted weaknesses by McGreivy and Hakim (2024) [23]. The existing methodology alleviates these concerns by keeping physical interpretability with closed-form conservation of norms and direct energy tracking, which offers clear standards on assessing the accuracy of models.

The periodic 2D system, whose probability norm was maintained at 98.7% and whose energy deviation was reduced to 1.1%, is also similar to nonconservative PDE quantum algorithms which were proposed by Sato *et al*. (2025) [19], where domains with variable parameters maintained 9799% stability even with spatial nonlinearity. These similarities also confirm that the current method of multidimensional systems can be scaled without losing much accuracy.

The same analytical formulation of this PPDE problem fits the principles of dynamical systems modeling given by Castillo (2025) [24] whose periodicity and boundary consistency constitute the long-term predictability of chaotic or oscillatory systems. Besides, the current results support the analytical validity of fractional and time-dependent PDE methods (Shakeel, Shah, and Chung, 2022) [25], which showed closed-form consistency to 98.9% in fractional domains - extremely comparable to the quantitative consistency here.

Lastly, the hybrid solver efficiency in retaining convergence in 200 fs is a positive indicator of a direct transition between classical numerical computation and new quantum PDEs algorithms as Hu *et al*. (2024) [16] and Sato *et al*. (2025) [19] describe. The achievement of the simulation to conserve energy within 1 percent and a norm deviation of less than + or -0.5 percent directly puts it in the position of the most numerically stable quantum-inspired solvers that have been reported in the literature over the last few years. Such results do not only confirm the construction of the suggested PPDE framework but also make it a viable numerical analog to simulate the future numerical solvers of quantum circuits solving PDEs, where norm conservation and error tolerance are important.

The results of this work support the new paradigm that quantum-inspired numerical simulations of PDEs, explicit and implicit, especially periodic and hybrid spectral algorithms, can obtain the stability and accuracy of near-quantum scales, and be run on classical computer equipment at computational scales. The model lies between a conventional PDE solver with the quantum-theoretical boundary definition of the PDE, making it suitable in bridging the gap that exists between a conventional PDE solver and quantum algorithmic frameworks and it can support the trajectories presented by Hu *et al*. (2024) [16], Garcia-Ripoll (2021) [14], and Huang *et al*. (2025) [18] to scalable, stable, and interpretable simulations of a PDE.

5. Conclusion

The current research has established the usefulness of quantum-inspired computational framework to model the time dynamics of the wave functions in one-dimensional partial differential equations. These findings proved the fact that the system remained at all times stable at norm and energy conservation at tolerable limits of a deviation of less than 1 and 0.5 respectively. This robust conservation tendency implies a great level of numerical stability and fidelity in the suggested hybrid Crank-Nicolson Spectral model. This drift in the energy observed of less than 0.9 percent and stability index of 99.4 percent confirm the strength of the discretization scheme and time-propagation scheme in the presence of periodic boundary conditions. The computation model was able to generate the oscillatory and dispersive properties of quantum wave dynamics at the expense of preserving probability density and numerical diffusion minimal over 200 femtoseconds (fs) of evolution. These findings confirm that the implemented algorithm is very effective in capturing dynamic characteristics of Schrodinger-type systems that have accuracy in both amplitude and phase tracking throughout the simulation domain. In addition, the framework also reduced the computational time by 31 percent relative to traditional finite-difference schemes at the same spatial accuracy (root mean square error less than 0.5 percent) and temporal accuracy (error propagation less than 1.2 percent). This performance shows that the solver developed is scaled and efficient on quantum-scale modeling on classical hardware.

Altogether, the current study develops a numerically justified foundation of quantum-inspired solvers in the PDEs field. Combining classical deterministic computation with quantum-enhanced principles of stability, the model has been introduced as a reliable and scalable basis to future high-dimensional and nonlinear simulations. The model is characterized by verifiable conservation of important physical quantities, which highlights potential applications of the model in the study of phenomena in the areas of quantum transport, nanoscale fluid dynamics and wave propagation among others. A more robust integration of variational quantum circuit or machine-learning-based optimizations will likely be the future of this research as it can help to further enhance the computational accuracy and efficiency.

References

1. Jin S, Liu N, Yu Y. Quantum simulation of partial differential equations: applications and detailed analysis. Physical Review A. 2023;108(3):032603.
2. Cao Y, Jin S, Liu N. Quantum simulation for time-dependent Hamiltonians with applications to non-autonomous ordinary and partial differential equations. Journal of Physics A: Mathematical and Theoretical. 2025;58(15):155304.
3. Tosti Balducci G, Chen B, Möller M, Gerritsma M, De Breuker R. Review and perspectives in quantum computing for partial differential equations in structural mechanics. Frontiers in Mechanical Engineering.

2022;8:914241.
4. Leong FY, Koh DE, Ewe WB, Kong JF. Variational quantum simulation of partial differential equations: applications in colloidal transport. International Journal of Numerical Methods for Heat & Fluid Flow. 2023;33(11):3669-3690.
5. Kocherla S, Song Z, Chrit FE, Gard B, Dumitrescu EF, Alexeev A, Bryngelson SH. Fully quantum algorithm for mesoscale fluid simulations with application to partial differential equations. AVS Quantum Science. 2024;6(3):031701.
6. Hu J, Jin S, Zhang L. Quantum algorithms for multiscale partial differential equations. Multiscale Modeling & Simulation. 2024;22(3):1030-1067.
7. Sato Y, Kondo R, Hamamura I, Onodera T, Yamamoto N. Hamiltonian simulation for hyperbolic partial differential equations by scalable quantum circuits. Physical Review Research. 2024;6(3):033246.
8. Yip C, Seol L, Hon XZ. A step-by-step approach to partial differential equations. Fusion of Multidisciplinary Research: An International Journal. 2022;3(1):302-315.
9. Wang S, Wang H, Perdikaris P. Learning the solution operator of parametric partial differential equations with physics-informed DeepONets. Science Advances. 2021;7(40):eabi8605.
10. Ganie AH, Sadek LH, Tharwat MM, Iqbal MA, Miah MM, Rasid MM, Osman MS. New investigation of the analytical behaviors for some nonlinear PDEs in mathematical physics and modern engineering. Partial Differential Equations in Applied Mathematics. 2024;9:100608.
11. Kocherla S, Song Z, Chrit FE, Gard B, Dumitrescu EF, Alexeev A, Bryngelson SH. Fully quantum algorithm for lattice Boltzmann methods with application to partial differential equations. arXiv preprint arXiv:2305.07148. 2023.
12. Oz F, San O, Kara K. An efficient quantum partial differential equation solver with Chebyshev points. Scientific Reports. 2023;13(1):7767.
13. Akinfe KT, Loyinmi AC. The implementation of an improved differential transform scheme on the Schrödinger equation governing wave-particle duality in quantum physics and optics. Results in Physics. 2022;40:105806.
14. García-Ripoll JJ. Quantum-inspired algorithms for multivariate analysis: from interpolation to partial differential equations. Quantum. 2021;5:431.
15. Hussein HH, Ahmed HM, Rabie WB, Ahmed KK, Hashemi MS, Bayram M. Multiple soliton solutions and other travelling wave solutions to new structured (2+1)-dimensional integro-partial differential equation using efficient technique. Physica Scripta. 2024;99(10):105270.
16. Hu J, Jin S, Liu N, Zhang L. Quantum circuits for partial differential equations via Schrödingerisation. Quantum. 2024;8:1563.
17. Ali R, Kumar D, Akguel A, Altalbe A. On the periodic soliton solutions for fractional Schrödinger equations. Fractals. 2024;32(7-8):2440033.
18. Huang S, Feng W, Tang C, He Z, Yu C, Lv J. Partial differential equations meet deep neural networks: a survey. IEEE Transactions on Neural Networks and Learning Systems. 2025;36(1):1-22.
19. Sato Y, Tezuka H, Kondo R, Yamamoto N. Quantum algorithm for partial differential equations of nonconservative systems with spatially varying parameters. Physical Review Applied. 2025;23(1):014063.
20. García-Molina P, Rodríguez-Mediavilla J, García-Ripoll JJ. Quantum Fourier analysis for multivariate functions and applications to a class of Schrödinger-type partial differential equations. Physical Review A. 2022;105(1):012433.
21. Ali R, Zhang Z, Ahmad H. Exploring soliton solutions in nonlinear spatiotemporal fractional quantum mechanics equations: an analytical study. Optical and Quantum Electronics. 2024;56(5):838.
22. Baleanu D, Karaca Y, Vázquez L, Macías-Díaz JE. Advanced fractional calculus, differential equations and neural networks: analysis, modeling and numerical computations. Physica Scripta. 2023;98(11):110201.
23. McGreivy N, Hakim A. Weak baselines and reporting biases lead to overoptimism in machine learning for fluid-related partial differential equations. Nature Machine Intelligence. 2024;6(10):1256-1269.
24. Castillo JCR. Differential equations: fundamentals, solution methods, and applications in dynamical systems and chaos theory. Ibero Ciencias-Revista Científica y Académica. 2025;4(2):22-42.
25. Shakeel M, Shah NA, Chung JD. Novel analytical technique to find closed form solutions of time fractional partial differential equations. Fractal and Fractional. 2022;6(1):24.
26. Stevens B, Colonius T. FiniteNet: a fully convolutional LSTM network architecture for time-dependent partial differential equations. arXiv preprint arXiv:2002.03014. 2020.
27. Jin S, Liu N, Ma C. Schrödingerization based computationally stable algorithms for ill-posed problems in partial differential equations. SIAM Journal on Scientific Computing. 2025;47(4):B976-B1000.